Error modeling and calibration of a 4RRR redundant positioning system

Sheng Yao, Xianmin Zhang, Jing Yu, and Benliang Zhu

Citation: AIP Advances **7**, 095009 (2017); doi: 10.1063/1.4993109
View online: http://dx.doi.org/10.1063/1.4993109
View Table of Contents: http://aip.scitation.org/toc/adv/7/9
Published by the American Institute of Physics

Error modeling and calibration of a 4RRR redundant positioning system

Sheng Yao, Xianmin Zhang,[a] Jing Yu, and Benliang Zhu
Guangdong Provincial Key Laboratory of Precision Equipment and Manufacturing Technology, School of Mechanical and Automotive Engineering, South China University of Technology, Guangzhou 510640, China

(Received 27 June 2017; accepted 4 September 2017; published online 12 September 2017)

Using the macro-micro combination positioning system for nanomanipulating can fulfill the requirements of large workspace, high precision and multi-degrees of freedom. As a macro part of the macro-micro combination positioning system, a redundantly actuated three degrees-of-freedom (DOF) parallel kinematic mechanism (4RRR) with a directly driven system is studied in this paper. Firstly, the error sensitivity of the 4RRR planar parallel mechanism is analyzed with global errors sensitive index (GESI) based on the error model of the positioning system. Then, a novel and practical calibration method combined with an error compensation strategy is proposed for the 4RRR positioning system. Finally, in order to verify the proposed method, a series of experiments are conducted with the laser measurement system in creditable conditions, and the data are illustrated for comparisons. The experimental results show that the positioning accuracy of the 4RRR positioning system is improved, and the performances of the end-effector are enhanced based on the proposed method.
[http://dx.doi.org/10.1063/1.4993109]

I. INTRODUCTION

Compared with the series robot, the virtues of the parallel mechanism (PM) are higher speed, stronger load capacity and better precision with small accumulative errors,[1–3] which is suitable for the multi-DOF precision positioning system. Based on planar parallel 3-DOF positioners, a macro-micro combination positioning system is established for nanoscale positioning.[4] As the macro part of the macro-micro combination positioning system, the 3-DOF PM has been delivered to fulfill micron grade positioning with the millimeter movement itinerary. Meanwhile, adding redundant kinematic chains or actuated joints for PMs can reduce the singularity inside the workspace and improve dynamic performance.[5,6] Fig. 1 shows two types of the macro-micro combination positioning systems, which both use PMs as the macro positioners. Based on a 3RRR PM (R represents the revolute pair and the underline of the R represents the actuated joint), a directly driven 4RRR PM is designed with an additional redundant kinematic chain, which is shown in Fig. 2.

However, the accuracy of actual 4RRR positioning system is always reduced due to processing error, assembly error and deformation of the 4RRR mechanism.[7–9] Kinematic calibration is one of the most widely used methods to improve the positioning accuracy of robots.[10–14] The calibration includes four steps: system error modeling, error measurement, parameter identification and error compensation.[15–17]

Afterward, sensitivity analysis can be carried out to estimate all geometric errors' influences on the end-effector based on the established error model. The GCI (Global Condition Index)[18] has been widely used in the traditional optimization, but it cannot reflect error sources along the kinematic

[a]Corresponding author: zhangxm@scut.edu.cn

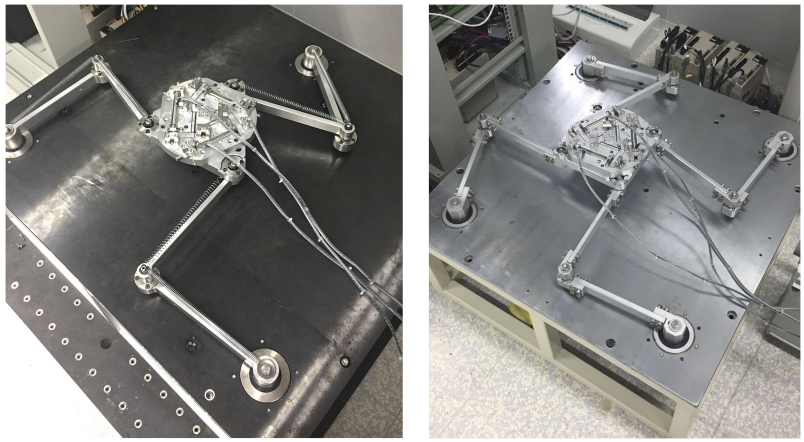

FIG. 1. Two types of the macro-micro combination positioning systems.

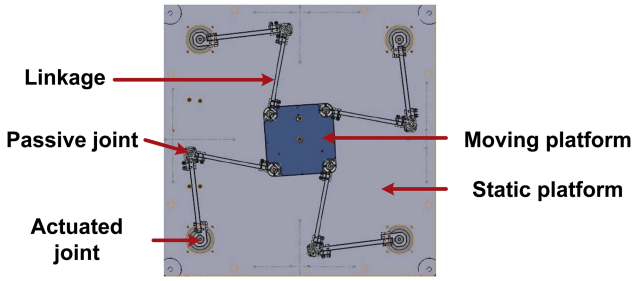

FIG. 2. The design diagram of 4RRR parallel mechanism.

chain. In addition, the GSI (global sensitivity index) has been introduced to analyze SCARA robots,[19] while the GESI (global errors sensitive index) has been involved in dealing with 3PRR PM,[20] but to the best knowledge of the authors, few published articles have been involved to analyze the error sensitivity of 4RRR PM at present.

Liu[21] introduces an approach to self-calibration for a type of redundant PM using measured information of the redundant kinematic chain. However, he only simulates his model and not all kinematic chains of his 4RRR model drive the end-effector, while we run the experiment based on our error model and all kinematic chains in our model are the same. Shao[22] identifies the parameters of his 3RRR parallel mechanism using wire sensors, but he do not consider the actuated joints errors, which we consider in our study. Ma[23] uses the algorithm of back propagation neural network for the external calibration of parallel mechanisms, but the errors of theoretical structural parameters were not taken into account.

A 4RRR PM is manufactured in our laboratory as the macro part of the macro-micro combination positioning system. In this paper, an error model of the directly driven 4RRR positioning system is derived. Based on this error model and Jacobian matrix, the GESI global errors sensitive index of the 4RRR manipulator is investigated in Section 2. Then, an external calibration method based on the decoupling error model and the compensation method is presented in Section 3. In Section 4 the calibration experiments are conducted, and the results are displayed directly. Finally, the conclusions of this paper are drawn in the last section.

II. ERROR MODELING AND ANALYSIS

A. Error modeling of the 4RRR mechanism

In this kind of 3-DOF redundant plane parallel mechanism, all kinematic chains are in the position control mode, so it is also called the directly driven 4RRR positioning system.

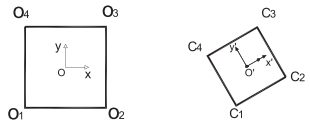

FIG. 3. Static and moving coordinate systems of 4RRR mechanism. (a) is the static platform, and (b) is the moving platform.

The coordinate systems for the 4RRR PM are created as shown in Fig. 3. The positioning system consists of a static platform (□ $O_1O_2O_3O_4$) and a moving platform (□ $C_1C_2C_3C_4$), which are connected by four branched chains. In order to compact the structure and improve the utilization of space, both the static platform and the moving platform use the square configuration, which is completely symmetric. The global Cartesian coordinate system O-XY is established on the static platform. Meanwhile, the moving coordinate system $O' - X'Y'$ is established on the moving platform.

As shown in Fig. 4, at the begin of kinematic chains, there are actuated joints O_n (n=1, 2, 3, 4) and the actuated angles α_1, α_2, α_3, $\alpha4$. Linkages O_nB_n and B_nC_n (n=1, 2, 3, 4) connect the static platform to the moving platform. Each kinematic chain contains two passive joints (B_n and C_n) and an actuated joint, which is connected to a servo motor. The length of linkages is respectively equal ($O_1B_1 = O_2B_2 = O_3B_3 = O_4B_4 = L_1$; $B_1C_1 = B_2C_2 = B_3C_3 = B_4C_4 = L_2$). L_4 and L_3 represent the circumradius of the static platform and moving platform respectively. Point M is the geometric center of the moving platform, which coincides with the origin of the moving coordinate O'. Then, the vector OM can be defined as the position of the end-effector (x, y, ϕ), where ϕ is formed by the positive direction of X-axis from the moving coordinate system and the static coordinate system. θ_1, θ_2, θ_3, θ_4 are the angles between the linkages B_1C_1, B_2C_2, B_3C_3, B4C4 and the positive direction of the X-axis. β_1, β_2, β_3, β_4 are the four angle parameters of the moving platform.

In the static coordinate system, the following equation of closed-loop vector is given according to kinematic chains.

$$\boldsymbol{O_nB_n + B_nC_n + O_nM + MO + OO_n = 0} \quad (n = 1, 2, 3, 4) \tag{1}$$

Expanding Eq. (1) into projections of two axes (X-axis, Y-axis), the kinematic model of the 4RRR is obtained as

$$\begin{cases} X_M = L_{n1}\cos\alpha_n + L_{n2}\cos\theta_n + L_{n3}\cos\gamma_n + X_{On} \\ Y_M = L_{n1}\sin\alpha_n + L_{n2}\sin\theta_n + L_{n3}\sin\gamma_n + Y_{On} \end{cases} \tag{2}$$

Where $\gamma_n = \beta_n + \phi$; $\beta_n = \frac{\pi}{4}(4n - 3)$, $(n = 1, 2, 3, 4)$; X_{On} and Y_{On} are related with L_{n4}.

A slight error δ is introduced at each error source as listed in Table I, and the kinematic model with errors is

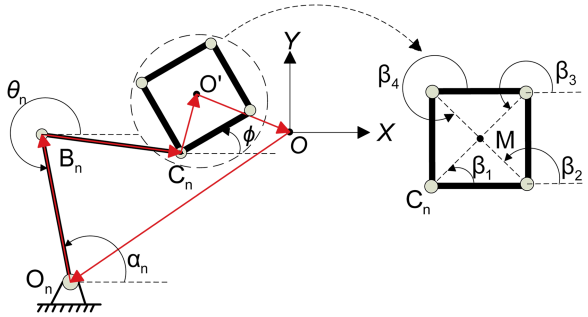

FIG. 4. Error modeling of the 4RRR planar parallel mechanism.

TABLE I. Description of error sources in 4RRR mechanism.

Error sources (n=1,2,3,4)	Description
$\delta\alpha_n$	Input errors of each actuated joint
δL_{n1}	Errors of each driving Linkage
δL_{n2}	Errors of each follower Linkage
δLn_3	Circumradius errors of the moving platform
$\delta\beta_n$	Angle errors of the moving platform
δX_{On}	Projection errors (X-axis) of the static platform circumradius
δY_{On}	Projection errors (Y-axis) of the static platform circumradius

$$\begin{cases} X_M + \delta x = (L_{n1} + \delta L_{n1})\cos(\alpha_n + \delta\alpha_n) + (L_{n2} + \delta L_{n2})\cos(\theta_n)... \\ ... + (L_{n3} + \delta L_{n3})\cos(\gamma_n + \delta\gamma_n) + (X_{On} + \delta X_{On}) \\ Y_M + \delta y = (L_{n1} + \delta L_{n1})\sin(\alpha_n + \delta\alpha_n) + (L_{n2} + \delta L_{n2})\sin(\theta_n)... \\ ... + (L_{n3} + \delta L_{n3})\sin(\gamma_n + \delta\gamma_n) + (X_{On} + \delta X_{On}) \end{cases} \tag{3}$$

where $\gamma_n + \delta\gamma_n = \beta_n + \delta\beta_n + \phi + \delta\phi \quad (n = 1, 2, 3, 4)$

According to the approximate formula $\begin{cases} \sin x \approx x \\ \cos x \approx 1 \end{cases} \quad (x << 1)$, higher-order terms are rounding off, and by Eq. (3) minus Eq. (2) the error model of 4RRR mechanism can be obtained as follows

$$\begin{aligned} &\delta x = -(L_{n1}\sin\alpha_n)\,\delta\alpha_n + (\cos\alpha_n)\,\delta L_{n2}... \\ &... - (L_{n3}\sin\gamma_n)\,\delta\gamma_n + (\cos\gamma_n)\,\delta L_{n3} + \delta X_{On} \end{aligned} \tag{4}$$

$$\begin{aligned} &\delta y = -(L_{n1}\cos\alpha_n)\,\delta\alpha_n + (\sin\alpha_n)\,\delta L_{n2}... \\ &... - (L_{n3}\cos\gamma_n)\,\delta\gamma_n + (\sin\gamma_n)\,\delta L_{n3} + \delta Y_{On} \end{aligned} \tag{5}$$

Where $\delta\gamma_n = \delta\beta_n + \delta\phi,\ (n = 1, 2, 3, 4)$.

As the position error (δx, δy) of the end-effector is coupling with the orientation error $\delta\phi$, for decoupling Eq. (4) is multiplied by $\cos\theta_n$ and Eq. (5) is multiplied by $\sin\theta_n$, (n=1, 2, 3, 4). Then an equation can be obtained as

$$\begin{cases} \cos\theta_n\delta x = \cos\theta_n\,[\,(L_{n1}\sin\alpha_n)\,\delta\alpha_n + (\cos\alpha_n)\,\delta L_{n1} + ... \\ ...(\cos\theta_n)\,\delta L_{n2} - (L_{n3}\sin\gamma_n)\,\delta\gamma_n + (\cos\gamma_n)\,\delta L_{n3} + \delta X_{On}\,] \\ \sin\theta_n\delta y = \sin\theta_n\,[\,(L_{n1}\cos\alpha_n)\,\delta\alpha_n + (\sin\alpha_n)\,\delta L_{n1} + ... \\ ...(\sin\theta_n)\,\delta L_{n2} - (L_{n3}\cos\gamma_n)\,\delta\gamma_n + (\sin\gamma_n)\,\delta L_{n3} + \delta Y_{On}\,] \end{cases} \tag{6}$$

By simplifying Eq. (6), the relation of input and output can transform into

$$\begin{aligned} &\cos\theta_n\delta x + \sin\theta_n\delta y - \delta L_{n3}\sin(\theta_n - \gamma_n)\delta\phi = ... \\ &...L_{1n}\sin(\theta_n - \alpha_n)\delta\alpha_n + .\cos(\theta_n - \alpha_n)L_{n1}\delta L_{n3} + \sin(\theta_n - \gamma_n)\delta\beta_n... \\ &... + \cos(\theta_n - \gamma_n)L_{n3} + \cos\theta_n\delta X_{On} + \sin\theta_n\delta Y_{On} + \delta L_{n2} \end{aligned} \tag{7}$$

Eq. (7) can also be written as a matrix form like

$$\delta\boldsymbol{X} = \boldsymbol{J_e}\delta\boldsymbol{d} \tag{8}$$

where

$$\delta\boldsymbol{d} = \left[\,\delta\boldsymbol{d}_1 \quad \delta\boldsymbol{d}_2 \quad \delta\boldsymbol{d}_3 \quad \delta\boldsymbol{d}_4\,\right]^T;$$

$$\delta \boldsymbol{d}_n = [\,\delta\alpha_n \quad \delta L_{n1} \quad \delta\beta_n \quad \delta L_{n3} \quad \delta X_{On} \quad \delta Y_{On} \quad \delta L_{n2}\,]^T;$$

$$\delta \boldsymbol{X} = \begin{bmatrix} \delta x & \delta y & \delta\phi \end{bmatrix}^T;$$

$$\boldsymbol{A_{nn}} = [\,L_{n1}\sin(\theta_n - \alpha_n) \quad \cos(\theta_n - \alpha_n) \quad L_{n3}\sin(\theta_n - \alpha_n)$$
$$\cos(\theta_n - \gamma_n) \quad \cos\theta_n \quad \sin\theta_n \quad 1\,] \quad (n = 1, 2, 3, 4);$$

$$\boldsymbol{J_1} = \begin{bmatrix} \cos\theta_1 & \sin\theta_1 & -L_{13}\sin(\theta_1 - \gamma_1) \\ \cos\theta_2 & \sin\theta_2 & -L_{23}\sin(\theta_2 - \gamma_2) \\ \cos\theta_3 & \sin\theta_3 & -L_{33}\sin(\theta_3 - \gamma_3) \\ \cos\theta_4 & \sin\theta_4 & -L_{43}\sin(\theta_4 - \gamma_4) \end{bmatrix}; \boldsymbol{J_2} = \begin{bmatrix} A_{11} & 0_{1\times7} & 0_{1\times7} & 0_{1\times7} \\ 0_{1\times7} & A_{22} & 0_{1\times7} & 0_{1\times7} \\ 0_{1\times7} & 0_{1\times7} & A_{33} & 0_{1\times7} \\ 0_{1\times7} & 0_{1\times7} & 0_{1\times7} & A_{44} \end{bmatrix}_{4\times28};$$

$$\boldsymbol{J_e} = (\boldsymbol{J_1^T J_1})^{-1}\boldsymbol{J_1^T J_2};$$

The matrix $\boldsymbol{J_e}$ is called the error transfer matrix since each element in the matrix $\boldsymbol{J_e}$ represents the contribution of each error source to the positioning error at the end-effector. Meanwhile, the matrix $\boldsymbol{J_e}$ can be used not only for analyzing the properties of the mechanism error transfer, but also for error identification.

B. Analysis of the error sources

For the calibration purpose, the most concerning factor is to find out the main error source, which will affect the positioning accuracy significantly. There are 28 error sources that would affect the positioning accuracy considering the error model of the 4RRR PM. Some error sources greatly affect the positioning accuracy, while contrastingly, the positioning accuracy is less sensitive to other error sources. According to the error transfer matrix $\boldsymbol{J_e}$, elements in matrix $\boldsymbol{J_e}$ determine the influence of the error source on the positioning accuracy. For example, the elements of the last row in $\boldsymbol{J_e}$ are the weights of the error source, and they determine the error sources in $\delta\alpha$ which will affect $\delta\phi$ mostly. That means the weight of the elements in the matrix $\boldsymbol{J_e}$ reflects the sensitivity of the error transfer. However, each positioning point has a $\boldsymbol{J_e}$, and the elements of matrix $\boldsymbol{J_e}$ would change at every point in the workspace area.

Accordingly, the local sensitivity coefficient of the error sources is obtained as

$$\boldsymbol{L}_{ij} = \left|\delta \boldsymbol{p}_{ij} \middle/ \delta \boldsymbol{X}\right| \quad (i = 1,2,3;\, j = 1\sim28) \tag{9}$$

Where $\delta \boldsymbol{p}_{ij} = \boldsymbol{J}_{eij} \cdot \delta \boldsymbol{d}$;

$\delta \boldsymbol{p}_{ij}$ is the transfer error on the end-effector based on the error source $\delta \boldsymbol{d}$. In order to obtain the maximum error in the whole working space, the sensitivity factor of error transfer is defined as:

$$\begin{aligned} GESI &= \iint_s \left|\delta \mathbf{p}_{ij} \middle/ \delta \mathbf{X}\right| ds \Big/ \iint_s ds \\ &= \iint_s \left[\left(\boldsymbol{J}_{eij} \cdot \delta \boldsymbol{d}\right) / \delta \boldsymbol{X}_i\right] ds \Big/ \iint_s ds \;, (i = 1,2,3;\, j = 1\sim28) \end{aligned} \tag{10}$$

where $\boldsymbol{J_{eij}}$ is not only the element of the error transfer matrix $\boldsymbol{J_e}$, but also the amplification factor of error sources. $\iint_s ds$ represents the whole workspace area.

In order to analyze the error sensitivity of 4RRR PM, the GESI is utilized and results of the calculation are given as follows. All angle errors and length errors are specified to be the same, and GESI of the 4RRR PM is shown in Fig. 5.

The above analysis shows that the sensitivity distribution tendency of all error sources is not exactly the same. At the X-DOF, the error mainly comes from the first and third kinematic chain. Meanwhile, the error at the Y-DOF mainly comes from second and fourth kinematic chain. However, at the rotational DOF, the error is the result of the interaction of all four kinematic chains. Although the distribution is not uniform, it can be found from the numerical analysis that the positioning errors of the 4RRR planar PM are basically from the input errors $\delta\alpha_n$ (n=1, 2, 3, 4) of the actuated joints. Which means, a small input error of the actuated joint will cause significant end-effector errors, and it must be identified and calibrated.

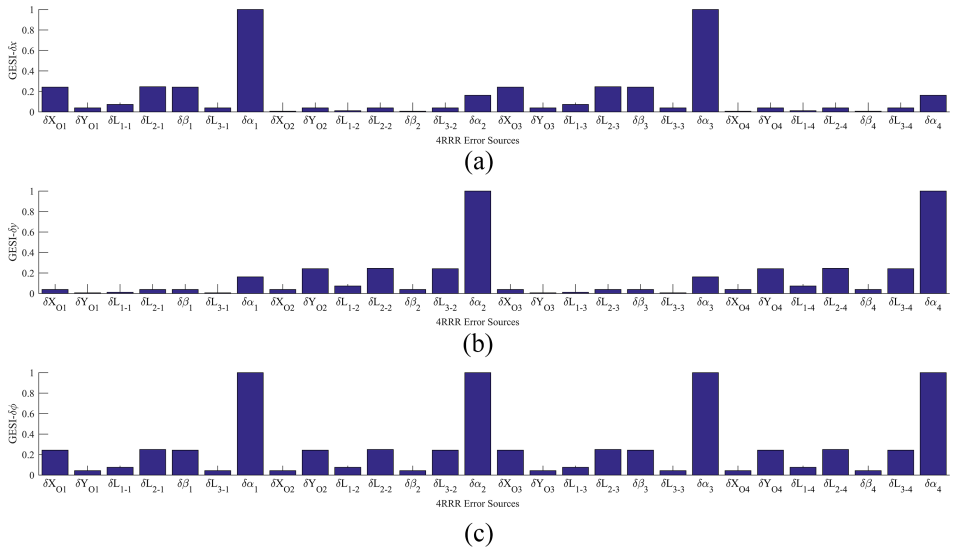

FIG. 5. The 4RRR GESI for error sources (Angle errors are all specified as 0.01°, length errors are all set as 0.01mm). (a) The GESI to the δx, (b) The GESI to the δy, (c) The GESI to the $\delta\phi$.

We can prove this conclusion by magnifying all angle errors five times in the GESI analysis, and the results are shown in Fig. 6.

When the length and angle errors are in the same order of magnitude, though the input errors from the actuated joints are high in GESI, other errors still have an impact on positioning accuracy. However, when angle errors enlarge, the effects of other errors are weakened, while the angle errors $\delta\alpha_n$ (n=1, 2, 3, 4) became the dominate factor of the positioning errors. Put it another way, these actuated joints errors play a significant role in the positioning errors of the 4RRR PM.

Moreover, the length errors of 4RRR are from manufacturing, while the angle errors $\delta\alpha_n$ (n=1, 2, 3, 4) result from the assembling. Which means, the angle errors $\delta\alpha_n$ (n=1, 2, 3, 4) are probably larger than the length errors in practical circumstances. Therefore, it can be concluded that the main error source for the 4RRR planar PM is the input error of actuated joints.

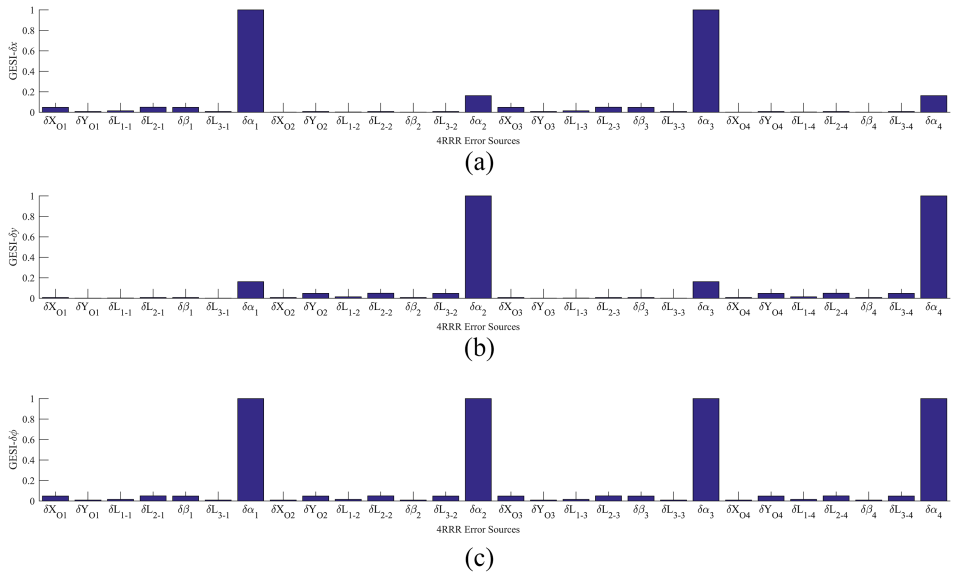

FIG. 6. The 4RRR GESI for error sources (Angle errors are all specified as 0.05°, length errors are all set as 0.01mm). (a) The GESI to the δx, (b) The GESI to the δy, (c) The GESI to the $\delta\phi$.

III. CALIBRATION METHOD

A. Calibration based on the 4RRR error model

The error sources mentioned above are induced during manufacturing or assembling. Although the error sources are hard to eliminate, they can still be identified and compensated.[24]

According to the error modeling, the error sources $\delta \boldsymbol{d}$ from kinematic chains can be identified, if the end-effector error $\delta \boldsymbol{X}$ is able to be measured by an external device. The parameters identification model of the 4RRR mechanism can be rewritten from its error model as

$$\delta \boldsymbol{d} = \boldsymbol{J}'_e \cdot \delta \boldsymbol{X} \tag{11}$$

where

$$\boldsymbol{J}'_e = \boldsymbol{J}_2^{-1} \cdot \boldsymbol{J}_1;$$

$$\boldsymbol{J}_1 = \begin{bmatrix} \cos\theta_1 & \sin\theta_1 & -L_{13}\sin(\theta_1-\gamma_1) \\ \cos\theta_2 & \sin\theta_2 & -L_{23}\sin(\theta_2-\gamma_2) \\ \cos\theta_3 & \sin\theta_3 & -L_{33}\sin(\theta_3-\gamma_3) \\ \cos\theta_4 & \sin\theta_4 & -L_{43}\sin(\theta_4-\gamma_4) \end{bmatrix}; \boldsymbol{J}_2 = \begin{bmatrix} A_{11} & 0_{1\times7} & 0_{1\times7} & 0_{1\times7} \\ 0_{1\times7} & A_{22} & 0_{1\times7} & 0_{1\times7} \\ 0_{1\times7} & 0_{1\times7} & A_{33} & 0_{1\times7} \\ 0_{1\times7} & 0_{1\times7} & 0_{1\times7} & A_{44} \end{bmatrix}_{4\times28};$$

$$\boldsymbol{A_{nn}} = [\, L_{n1}\sin(\theta_n-\alpha_n) \quad \cos(\theta_n-\alpha_n) \quad L_{n3}\sin(\theta_n-\alpha_n) \quad \cos(\theta_n-\gamma_n) \quad \cos\theta_n \quad \sin\theta_n \quad 1\,] \quad (n=1,2,3,4);$$

$$\delta \boldsymbol{d} = \begin{bmatrix} \delta \boldsymbol{d}_1 & \delta \boldsymbol{d}_2 & \delta \boldsymbol{d}_3 & \delta \boldsymbol{d}_4 \end{bmatrix}^T;$$

$$\delta \boldsymbol{X} = \begin{bmatrix} \delta x & \delta y & \delta \phi \end{bmatrix}^T;$$

By measuring the end-effector errors from multiple points in the workspace, all the errors sources ($\delta\alpha_n$, δL_{n1}, δL_{n2}, δL_{n3}, $\delta\beta_n$, δX_{An}, δY_{An}) can be identified. The kinematic calibration process is carried out as the follows:

Step 1. A static coordinate system is established based on the positioning holes on the moving platform and the static platform with a laser tracker. The measuring points are distributed in the workspace, and each point is separated in 20 mm intervals. We define the number of measuring points as m. Theoretically, the more the measuring points calculated, the more solvable the overdetermined equations are.

Step 2. Using the directly driven 4RRR positioning system and the guide of the laser tracker, the centroid of the end-effector coincides with the origin of the coordinate system. As the 0° attitude angle has a better condition number of the Jacobian matrix, the end-effector keeps 0° attitude angle during the calibration process.

Step 3. Using the positioning system to control the movement of the end-effector to the measuring point (x_j, y_j, ϕ_j) (j=1~m). When the moving platform is stable, the laser tracker is used to measure the centroid of the moving platform O_1' (x'_{j1}, y'_{j1}, ϕ'_{j1}) (j=1~m) and another point O_2' (x'_{j2}, y'_{j2}, ϕ'_{j2}) (j=1~48), which is at the X-axis of the moving coordinate.

Step 4. Repeat Step 2 and Step 3 until achieving the required numbers of measuring points.

Step 5. The attitude error of the end-effector is calculated by Equation (12). Eventually, the parameters of the model are identified by the least square method.

$$\begin{cases} \delta x = x'_{j1} - x_j \\ \delta y = y'_{j1} - y_j \\ \delta \phi = \mathrm{sgn}(y'_{j2} - y'_{j1})\cos^{-1}\left|(x'_{j2} - x'_{j1}) \Big/ \sqrt{(x'_{j2} - x'_{j1})^2 + (y'_{j2} - y'_{j1})^2}\right| \end{cases} \tag{12}$$

B. Error compensation strategy

The inverse distance method[25,26] can be used for interpolation. In this paper, the interpolation method is used to predict the error distribution within the workspace, based on the end-effector error at those limited numbers of measuring points. Continually, those corresponding errors are compensated to the joint space in order to complete the error compensation.

As mentioned earlier, the measuring point is defined as (x_j, y_j, ϕ_j) $(j=1\sim m)$, and a target point is defined as (x_0, y_0, ϕ_0) within the workspace. If the target point is one of the measuring points, then the error value of the target point equals to the error of this measuring point. Otherwise, the error value of the target point is calculated as

$$\begin{cases} \delta x_0 = \sum_{j=1}^{48} z_j \delta x_j \\ \delta y_0 = \sum_{j=1}^{48} z_j \delta y_j \\ \delta \phi_0 = \sum_{j=1}^{48} z_j \delta \phi_j \\ z_j = f(d_j) \Big/ \sum_{j=1}^{48} f(d_j) \\ f(d_j) = 1 \Big/ d_j^3 \end{cases} \tag{13}$$

where δx_0, δy_0 and ϕ_0 are the errors of the target point (x_0, y_0, ϕ_0), z_j is the weight of measuring points (x_j, y_j, ϕ_j) $(j=1\sim m)$, and d_j is the distance between the target point and those measuring points.

With this interpolation method, errors at all points within the workspace of 4RRR PM can be compensated. By the distance inverse ratio method, further measuring points will have a weakened influence to the target point, while closer measuring points will strongly influence the target point. In the calibration, the positioning errors of the end-effector at non-measuring points can be obtained by this compensation strategy, which can highly improve the efficiency of error calibration in the workspace of the positioning system.

IV. EXPERIMENTAL STUDIES

A. Experimental system description

In this section, the calibration experiment based on the error model described in the previous section is carried out.

The control system of 4RRR PM based on position control mode is developed as shown in Fig. 7. This experimental system consists of an IPC (Industrial Personal Computer), a motion control card, the AC servo system, the planar parallel mechanism and a laser tracker. The industrial personal computer contains human-computer interaction interface, comprised of a host, a display, a mouse and a keyboard, which is also used to write C# program in Visual Studio. The motion control card is DMC-1846 high-performance motion control card produced by the Galil Company. DMC-1846 provides a communication driver library supported on the. NET, which will be convenient for the researcher to do the secondary development. The positioning system consists of four independent AC servo system, which all are Yaskawa V series servo systems. Each Yaskawa servo system contains an SGMAV-120A servo driver, a reducer, a 20-bit incremental encoder and an SGMAV-10ADA61 servo motor, which can provide 3000 r/min speed and 9.55 N/m torque.

Fig. 8 shows the instructions passing process of the experimental system. The self-developed C# control software uses the specific control algorithm to calculate the control inputs, and the control inputs are converted into the voltage signal which is output to the servo drivers through the D/AC

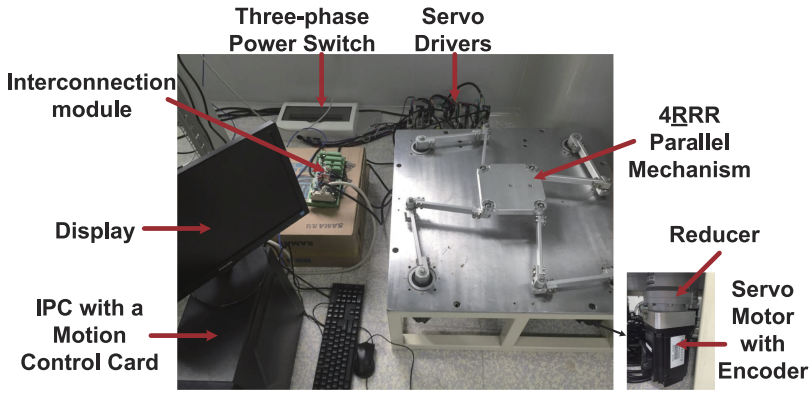

FIG. 7. The directly driven 4RRR positioning system.

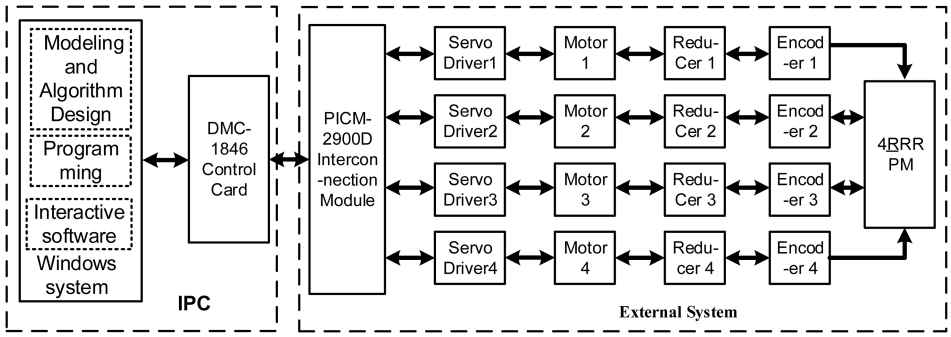

FIG. 8. Control block diagram of the experimental system.

interface. The motor driver amplifies the received DC reference voltage signal and converts it into a high frequency and high voltage AC drive voltage, which is inputted to the servo motors. Then the motor will adjust the velocity and displacement of the actuated joints, and finally the end-effector positioning is completed through the kinematic chains. The encoders send information of the actual displacement and velocity to the motion control card as feedbacks.

In our calibration, we use a laser tracker as the external measuring device. As shown in Fig. 9, this laser tracker measurement system is Leica AT901-B with the 0.01μm resolution and 10μm precision, and the tracking speed is up to 6 m/s to fulfill the requirement of the calibration experiment. The specific information of the experimental equipment is listed in the following Table II.

As the measurement device of this 4RRR positioning system, the laser tracker measurement system must have good repeatability. In order to test the real repeatability of the measurement device, a position of the end-effector is measured for 247 times using the Leica AT901-B system. According

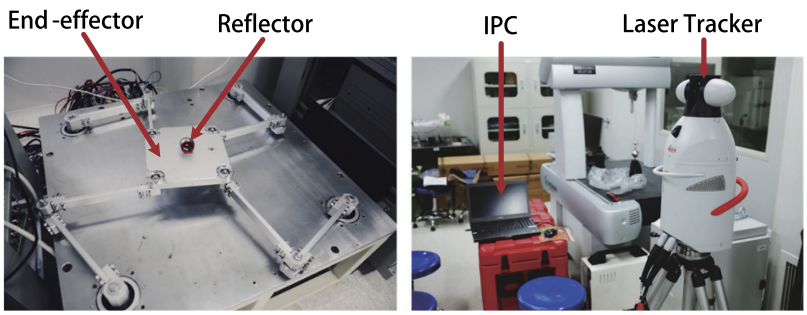

FIG. 9. The Leica measurement system.

TABLE II. The directly driven 4RRR positioning system.

Name	Model	Description
Measuring equipment	Leica AT901-B	0.01μm resolution, 10μm precision and 50m measuring range
Data acquisition software	Spatial Analyzer	Data acquisition software of laser tracker
Servo system	Yaskawa V series	3000 r/min speed with 20-bit incremental encoder
Control card	DMC-1846	4 axis motion control card
Software for programming and control	Microsoft Visual Studio 2015	Secondary development combined C# and GalilTools

to the test data as shown in Fig. 10, the repeated measurement accuracy is within the range of ±4 μm in the X direction, ± 3 μm in the Y direction, and ± 2 μm in the Z direction. The standard deviations of measurement results on each direction are 1.048 μm (X-axis), 1.071 μm (Y-axis), 0.759 μm

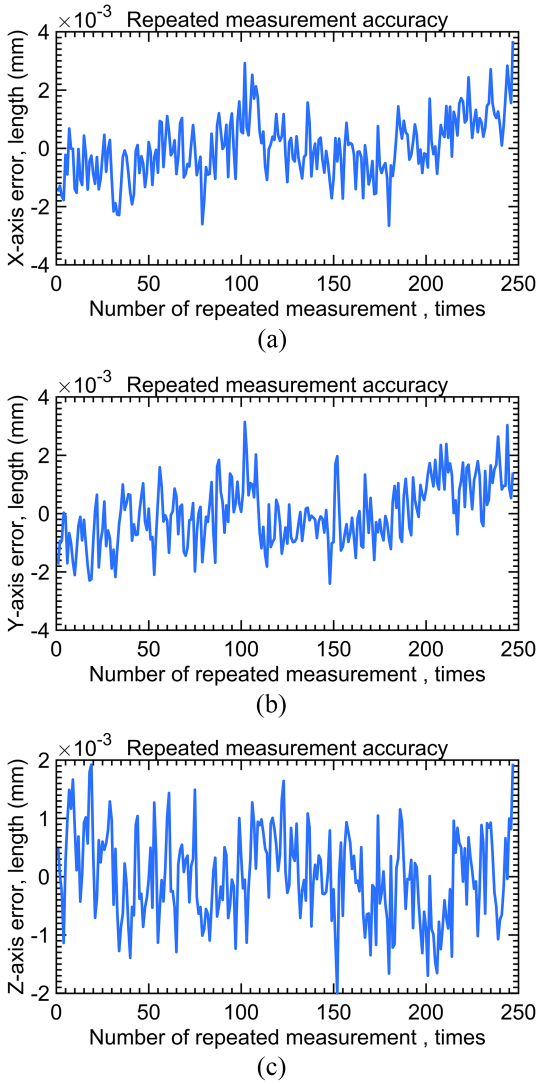

FIG. 10. Repeatability of Leica AT901-B system. (a) Repeatability of measurement system on X-axis, (b) Repeatability of measurement system on Y-axis, (c) Repeatability of measurement system on Z-axis.

(Z-axis) respectively. This indicates that the Leica AT901-B system has excellent repeatability and it is capable of measuring the pose of 4RRR PM in our calibration study.

B. Experiments and discussion

The theoretical length parameters of our 4RRR PM are L_1=245.00 mm, L_2=242.00 mm, L_3=112.00 mm, and L_4=400.00 mm, which has been manufactured based on the optimal design criteria.[27] The theoretical workspace of 4RRR PM is a square like area, and the radius of its inscribed circle is $L_1 + L_2 + L_3 - L_4 = 199$ mm. However, in real applications, mechanisms are not operated in the whole workspace, but within a small region.[28] In this calibration experiment, a square area with dimension 160 mm × 160 mm is selected as shown in Fig. 11, and the matrix $\boldsymbol{J_e}$ of the 4RRR PM enjoys good condition numbers in this area. 48 measuring points within this workspace are chosen as shown in Fig. 12.

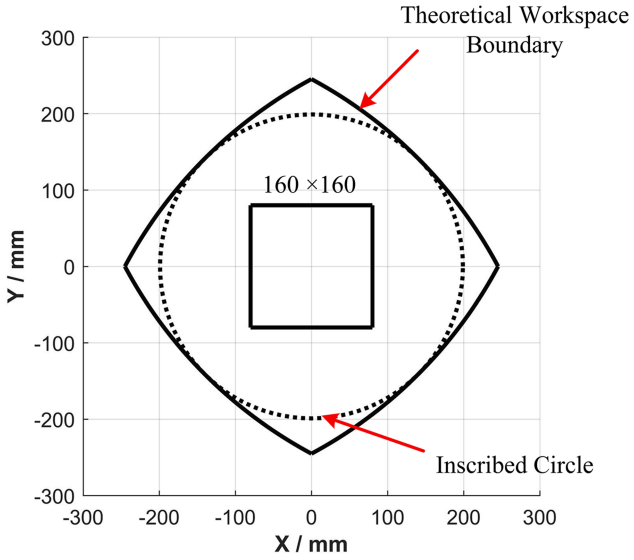

FIG. 11. Workspace of the 4RRR parallel manipulator.

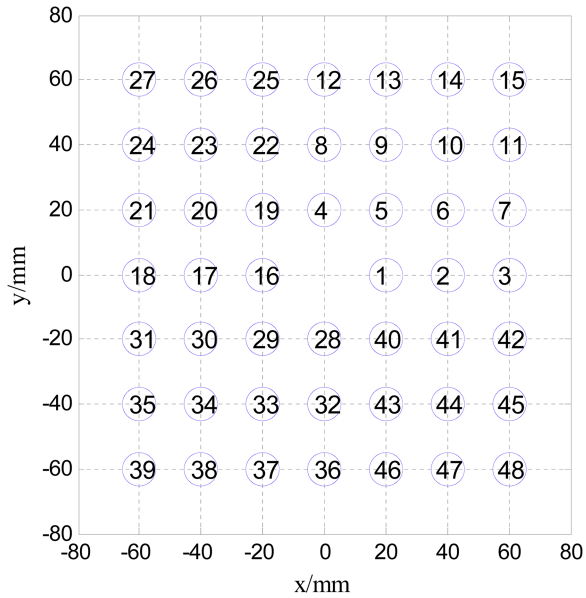

FIG. 12. Distribution of measuring points.

Since positioning repeatability is one of the significant indexes to evaluate the overall performance of a positioning system, it is important to investigate the repeatability of the 4RRR positioning system before the calibration. A repeated positioning experiment is conducted based on ISO 9283:1998 standard with Keyence LK-H050 laser displacement sensor, which has higher measuring accuracy (±2 μm) and excellent measuring repeatability (0.025 μm). According to ISO 9283:1998, the

TABLE III. Repeatability of 4RRR PM.

Test point	RP (mm)	Test point	RP (mm)
P_1	0.0017 ± 0.0072	P_4	0.0039 ± 0.0114
P_2	0.0030 ± 0.0116	P_5	0.0040 ± 0.0146
P_3	0.0033 ± 0.0114	P_6	0.0031 ± 0.0117

TABLE IV. Identified parameters.

Errors	Chain 1	Chain 2	Chain 3	Chain 4
$\delta\alpha_i$/mrad	0.0029	-0.0014	-0.0055	-0.0012
δL_{i1}/μm	0.1426	0.3109	-0.4371	-0.2113
δL_{i2}/μm	-0.0037	0.0008	0.0106	0.0023
δL_{i3}/μm	0.2472	-0.1441	-0.2861	-0.0728
$\delta\beta_i$/mrad	0.1748	0.0807	0.2024	-0.0515
δX_{Oi}/μm	0.1748	0.0087	0.2022	0.0515
δY_{Oi}/μm	0.1219	-0.0707	-0.1332	-0.0199

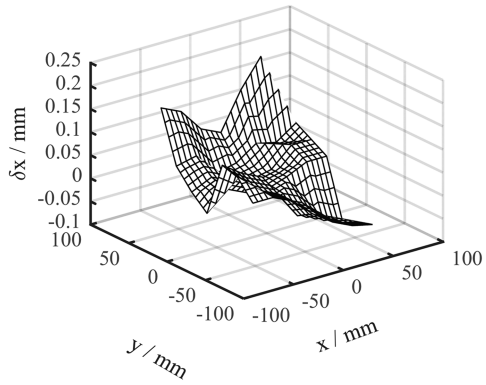

(a)

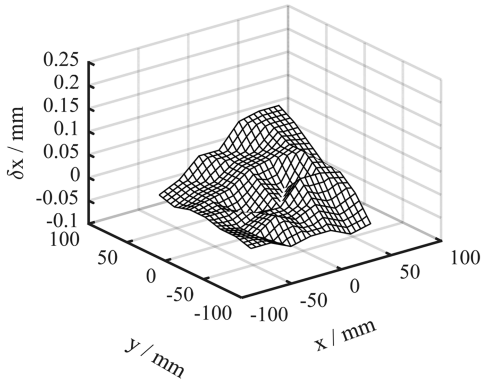

(b)

FIG. 13. δx distribution. (a) Before calibration, (b) After calibration.

end-effector is cyclically moved from test points P_6 to P_1 for 30 times, and the distance between two adjacent points is 1 mm. By experiment data and following equations, the repeated positioning (RP) accuracy is obtained as shown in Table III.

$$RP = \bar{l} \pm 3S \tag{14}$$

$$\bar{l} = \frac{1}{n}\sum_{j=1}^{n} l_j \tag{15}$$

$$S = \sqrt{\frac{\sum_{j=1}^{n}\left(l_j - \bar{l}\right)^2}{n-1}} \tag{16}$$

These results of the repeated positioning experiment show that the largest repeated positioning error among test points is 0.0040 ± 0.0146 mm. Though random errors would affect the positioning system, the repeatability of 4RRR positioning system is acceptable and relatively low compared with the size of 4RRR PM.

The world frame is established based on the location holes, and the zero position of the end-effector is also confirmed by these location holes on both moving platform and the base. before our calibration process the plane of the moving platform has been fitted in the laser measurement system by selecting multiple points on the surface in order to minimize the deviation of the end-effector on Z-direction, and the moving coordinate O′X′Y′ is established based on this fitting plane X′Y′.

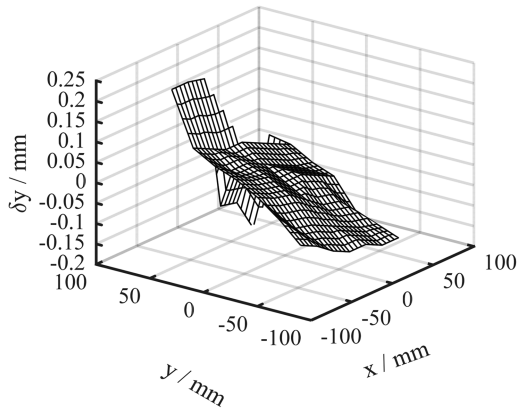

(a)

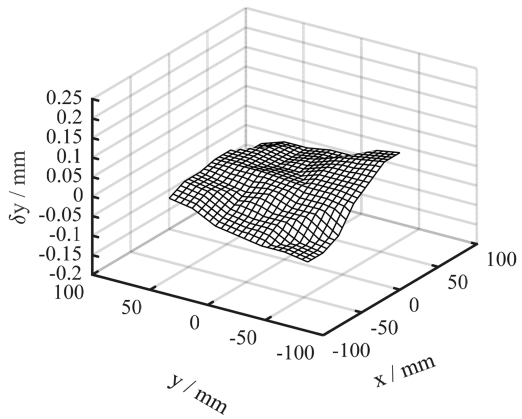

(b)

FIG. 14. δy distribution. (a) Before calibration, (b) After calibration.

According to the calibration process mentioned in previous sections, the experimental data are acquired by a Leica AT901-B laser tracker. To minimize the introduction of external errors, the end-effector returns home by the guide of the laser tracker. The experimental procedure can be described as: Moving the end-effector to the measuring point; measuring the positioning errors of the end-effector; identifying the parameters through the model; and returning home. By repeating the above procedure, all the information of measuring points is collected and then the parameters of the system can be calculated. Based on the experimental data of the measured errors, the identified parameters are obtained as shown in Table IV.

The identified parameters of input errors $\delta\alpha_i$ cannot be neglected since the end-effector errors are more sensitive to error sources $\delta\alpha_i$ as shown in Figs. 5 and 6. Meanwhile, smaller $\delta\alpha_i$ can avoid the overcorrection after the compensation. By substituting the identified parameters into the compensation method, the 4$\underline{\text{R}}$RR parallel mechanism has been measured again by the laser tracker after the compensation. The results of the error distributions are plotted in Fig. 13, Fig. 14 and Fig. 15.

The positioning error of the end-effector is within the range of -0.08~0.21 mm at the X-axis of the workspace and within the range of -0.17~0.22 mm at the Y-axis according to the data of the error distributions. The figures above show that the end-effector error is larger at the boundary of measuring area. This phenomenon conforms to the properties of the parallel mechanism. The further the end-effector moves away from the origin point, the closer to the singular boundary it is. Therefore the end-effector error becomes larger when it is near the singular boundary. After the calibration, the end-effector error drops to -0.08 ~0.08 mm at the X-axis and -0.09~0.05mm at the Y-axis. In addition, the attitude error of the end-effector falls from 0.30° to 0.14°. Meanwhile, all

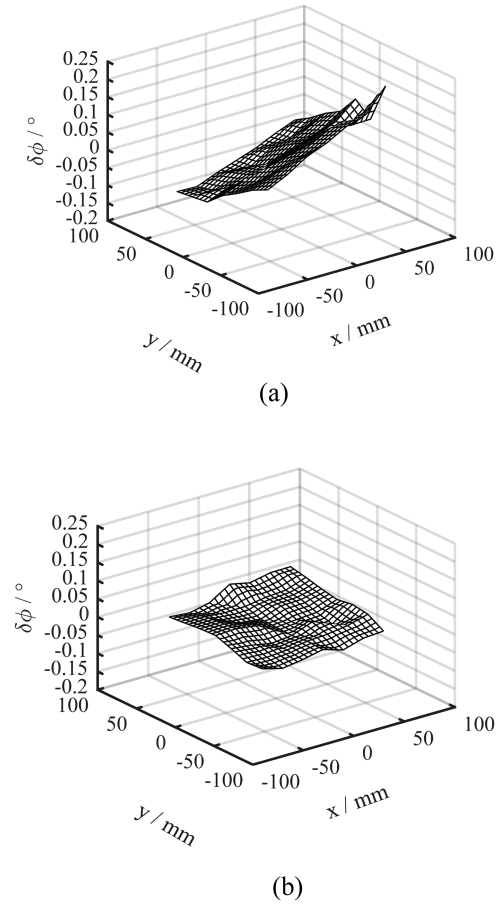

FIG. 15. $\delta\phi$ distribution. (a) Before calibration, (b) After calibration.

the distributions of the end-effector errors convert to a flat shape, and the end-effector appears better positioning performance near the origin point. Furthermore, the error distributions become more homogeneous, and the extreme values of the positioning errors decrease rapidly. The positioning accuracy of 4RRR redundant planar mechanism has dramatically improved in all DOF of the end-effector as shown in Table V. The positioning error of the 4RRR mechanism becomes less than 0.09 mm in a cubic workspace with the side length of 160 mm, and the effectiveness of the calibration method is verified.

TABLE V. The comparison of the end-effector errors.

Error	Before calibration	After calibration	Percentage reduction
δx	-0.08 ~ 0.21 mm	-0.08 ~ 0.08 mm	44.8%
δy	-0.17 ~ 0.22 mm	-0.09 ~ 0.05 mm	64.1%
$\delta\phi$	0.30°	0.14 °	53.3%

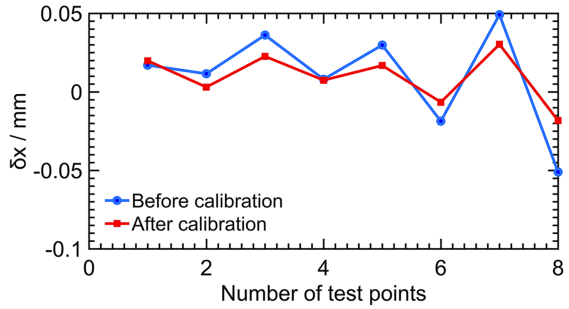

(a)

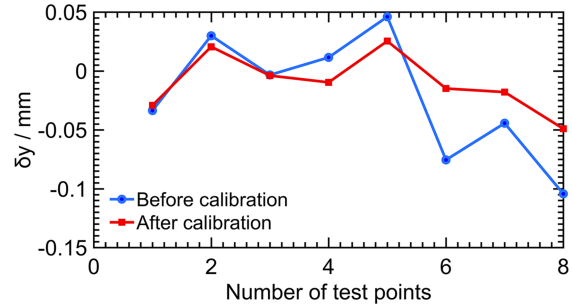

(b)

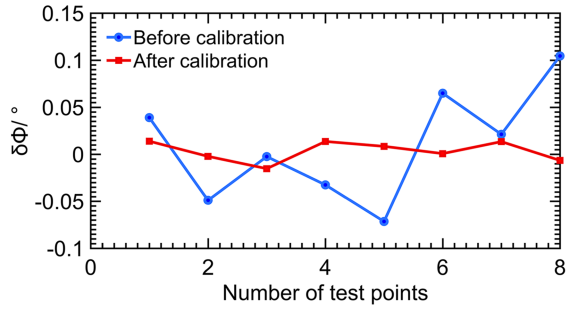

(c)

FIG. 16. Experiment of evaluating error compensation. (a) Errors of end-effector on X-direction, (b) Errors of end-effector on Y-direction, (c) Errors of end-effector on ϕ-direction.

To evaluate the compensation strategy, an additional experiment is conducted with the test points which are different from those used in the identification (P_1(30, 0), P_2(0, 30), P_3 (30, 30), P_4 (-30, 0), P_5 (-30, 30), P_6 (0,-30), P_7 (-30, -30), P_8 (30, -30)). The results are plotted in Fig. 16. It can be inferred that after the calibration the positioning errors generally decrease, and the peak value of errors reduces dramatically. This indicates that the error compensation method is effective, and it can be commonly used in PMs calibrations.

V. CONCLUSION

In this paper, an error model of a 4RRR redundant planar parallel mechanism is established. We analyze the error sensitivity of the 4RRR PM with the global errors sensitive index and conclude that the main error source for the 4RRR planar PM is the input error of actuated joints. A practical calibration method combined an error compensation strategy are proposed based on the single measurement apparatus with limited-DOF measuring ability. The repeatability of both 4RRR positioning system and the laser measurement system is tested by experimental methods, and the data show that both systems are capable of conducting calibration experiments. Then, In order to verify the proposed calibration method, the experimental study of the 4RRR positioning system is conducted, and the error sources are identified with laser measurement system. Moreover, we made a comparison between the distributions of the end-effector errors before calibration and after calibration based on the experimental data. The results show that the proposed methods can improve the positioning accuracy of the 4RRR positioning system, and the end-effector gives better performances within the workspace.

For future investigations, the calibration of non-geometrical parameters such as gear clearances and joint clearance should be taken into account in order to further improve the positioning accuracy.

ACKNOWLEDGMENTS

This work was supported by the National Natural Science Foundation of China (U1501247) and the Science and Technology Research Projects of Guangdong Province (2014B090917001, 2015B020239001). The authors gratefully acknowledge these support agencies.

[1] T. Lung-Wen. *Robot analysis, "the mechanics of serial and parallel manipulators,"* John Wiley & Sons, (1999).
[2] J. P. Merlet, "Jacobian, manipulability, condition number, and accuracy of parallel robots," Journal of Mechanical Design **128**(1), 199–206 (2006).
[3] X. Chen, F. Gao, C. Qi, X. Tian, and L. Wei, "Kinematic analysis and motion planning of a quadruped robot with partially faulty actuators," Mechanism and Machine Theory **94**, 64–79 (2015).
[4] R. Wang and X. Zhang, "Optimal design of a planar parallel 3-DOF nanopositioner with multi-objective," Mechanism and Machine Theory **112**, 61–83 (2017).
[5] D. Liang, Y. Song, T. Sun, and G. Dong, "Optimum design of a novel redundantly actuated parallel manipulator with multiple actuation modes for high kinematic and dynamic performance," Nonlinear Dynamics **83**(1-2), 631–658 (2016).
[6] J. P. Merlet, "Redundant parallel manipulators," Laboratory Robotics and Automation **8**(1), 17–24 (1996).
[7] A. Joubair, M. Slamani, and I. A. Bonev, "Kinematic calibration of a 3-DOF planar parallel robot," Industrial Robot: An International Journal **39**(4), 392–400 (2012).
[8] H. N. Nguyen, J. Zhou, and H. J. Kang, "A calibration method for enhancing robot accuracy through integration of an extended Kalman filter algorithm and an artificial neural network," Neurocomputing **15**, 996–1005 (2015).
[9] G. Du, P. Zhang, and D. Li, "Online robot calibration based on hybrid sensors using Kalman Filters," Robotics and Computer-Integrated Manufacturing **31**, 91–100 (2015).
[10] T. Huang, D. G. Chetwynd, D. J. Whitehouse, and J. Wang, "A general and novel approach for parameter identification of 6-DOF parallel kinematic machines," Mechanism and Machine Theory **40**(2), 219–239 (2005).
[11] M. To and P. Webb, "An improved kinematic model for calibration of serial robots having closed-chain mechanisms," Robotica **30**(6), 963–971 (2012).
[12] A. Joubair and I. A. Bonev, "Kinematic calibration of a six-axis serial robot using distance and sphere constraints," The International Journal of Advanced Manufacturing Technology **77**(1-4), 515–523 (2015).
[13] T. Huang, D. J. Whitehouse, and D. G. Chetwynd, "A unified error model for tolerance design, assembly and error compensation of 3-DOF parallel kinematic machines with parallelogram struts," CIRP Annals-Manufacturing Technology **51**(1), 297–301 (2002).
[14] J. Zhang, Q. Chen, C. Wu, and Q. Li, "Kinematic calibration of a 2-DOF translational parallel manipulator," Advanced Robotics **28**(10), 707–714 (2014).
[15] S. K. Saha, *Introduction to robotics* (Tata McGraw-Hill Education, 2014).
[16] T. Huang and D. J. Whitehouse, "A simple yet effective approach for error compensation of a tripod-based parallel kinematic machine," CIRP Annals-Manufacturing Technology **49**(1), 285–288 (2000).

[17] P. Xie, Z. J. Liu, and Y. H. Du, "Error compensation method of parallel robot based on ant colony algorithm," Computer Engineering **16**, 006 (2011).
[18] J. Angeles and C. Gosselin, "A global performance index for the kinematic optimization of robotic manipulators," Journal of Mechanical Design **113**(3), 220–226 (1991).
[19] Y. Chen, F. Xie, X. Liu, and Y. Zhou, "Error modeling and sensitivity analysis of a parallel robot with SCARA (selective compliance assembly robot arm) motions," Chinese Journal of Mechanical Engineering **27**(4), 693–702 (2014).
[20] J. S. Mo, Z. C. Qiu, L. Zeng, and X. M. Zhang, "A new calibration method for a directly driven 3PRR positioning system," Journal of Intelligent and Robotic Systems **85**(3-4), 613–631 (2017).
[21] D. Liu, L. Wang, and Y. Peng, "Self-calibration of a class of parallel kinematic machines with redundant kinematic chain," Chinese Journal of Mechanical Engineering **48**(1), 1–6 (2012).
[22] Z. Shao, X. Tang, and L. Wang, "Self-calibration method of planar flexible 3-RRR parallel manipulator," Chinese Journal of Mechanical Engineering **45**(3), 150–155 (2009).
[23] L. Ma, Y. J. Yu, W. M. Cheng, W. B. Rong, and L. N. Sun, "Positioning error compensation for a parallel robot based on BP neural networks," Optics and Precision Engineering **5**, 018 (2008).
[24] P. H. Hi and K. P. Song, "The structure parameter calibration of a planar 3RRR manipulator," Manufacturing Automation **10**, 009 (2005).
[25] J. Guodong, L. Yancong, and N. Wenjie, "Comparison between inverse distance weighting method and Kriging," Journal of Changchun University of Technology **24**(3), 53–57 (2003).
[26] A. J. Patel and K. F. Ehmann, "Calibration of a hexapod machine tool using a redundant leg," International Journal of Machine Tools and Manufacture **40**(4), 489–512 (2000).
[27] F. Gao, X. J. Liu, and X. Chen, "The relationships between the shapes of the workspaces and the link lengths of 3-DOF symmetrical planar parallel manipulators," Mechanism and Machine Theory **36**(2), 205–220 (2001).
[28] X. Zhang and X. Zhang, "A comparative study of planar 3-RRR and 4-RRR mechanisms with joint clearances," Robotics and Computer-Integrated Manufacturing **40**, 24–33 (2016).